Wave-4 Pattern of the Equatorial Mass Density Anomaly - A thermospheric signature of tropical deep convection

Huixin Liu

Research Institute for Sustainable Humanosphere, Kyoto University, Japan

Mamoru Yamamoto

Research Institute for Sustainable Humanosphere, Kyoto University, Japan

Hermann Lühr

Helmholtz Centre Potsdam, GFZ German Research Centre for Geosciences, Potsdam, Germany

H. Liu, M. Yamamoto Research Institute for Sustainable Humanosphere, Kyoto University, Uji 611-0011, Japan (huixin@rish.kyoto-u.ac.jp)

H. Lühr, Helmholtz Centre Potsdam, GFZ German Research Centre for Geosciences, D-14473 Potsdam, Germany

The equatorial mass density anomaly (EMA) is an anomalous latitudinal distribution of the atmospheric mass density, with its equinox configuration consisting of a density trough near the Earth's dip equator flanked by density crests around $\pm 25°$ dip latitude. As a novel feature, this study it reveals a pronounced 4-peak longitudinal pattern of the EMA, which is in reminiscence of the wave-4 like structure in the neutral wind and the equatorial ionization anomaly (EIA). It is found that the wave-4 modulation in the EMA trough region is in phase with that in the EMA crest region, in contrast to the $180°$ phase reversal for the case of EIA. This difference strongly suggest that although the latitudinal structure of the EMA is principally caused by the EIA via ion drag, its wave-4 pattern likely arises from different sources. The direct penetration of the non-migrating diurnal tides DE3 to the F-region height or thermal budget modulation by the composition NO at lower thermosphere are discussed as plausible candidates. Our results reveal a 4-hour phase lag between the wave-4 patterns in neutral density and wind, and a 2% peak-to-peak amplitude of the neutral density wave-4 pattern. These results find good agreements with theoretical predictions based on direct penetration of the DE3 to F-regions heights, hence strongly support this mechanism. Our observations thus add further evidence for the influence of tropical deep convection on the thermospheric dynamics.

1. Introduction

The equatorial mass density anomaly (EMA) is an interesting and important feature of the Earth's thermosphere in tropical regions, first observed by the CHAMP satellite [*Liu et al.*, 2005]. It is an anomalous latitudinal distribution of the atmospheric mass density, with its equinox configuration consisting of a density trough near the Earth's dip equator flanked by density crests around $\pm 25^{\circ}$ dip latitude. This structure is the neutral counterpart of the well-known equatorial ionization anomaly (EIA) in the ionosphere, which has been recognized and studied since the 1930s [*Appleton*, 1946; *Balan and Bailey*, 1995]. The EMA has been proposed to form primarily under the influence of EIA via ion drag, with some contribution from chemical heating fuelled by charge exchange between O^+ and O_2 or N_2 [*Liu et al.*, 2005]. It resembles fairly well the EIA in many climatological aspects, e.g., the seasonal and solar cycle variations [*Liu et al.*, 2007].

Recently the EIA has been revealed to exhibit a wave-4 longitudinal variation, which closely resembles the land-ocean distribution [e.g. *Sagawa et al.*, 2005; *Immel et al.*, 2006; *Wan et al.*, 2008]. It is now generally accepted that this structure forms as an effect of the E-region dynamo modulation by the eastward propagating non-migrating diurnal tide with wavenumber 3 (DE3) [*Immel et al.*, 2006; *Hagan et al.*, 2007; *Jin et al.*, 2008]. When viewed at one fixed local time from slowly precessing satellites, this feature manifests as a 4-peak structure. On the other hand, thermospheric neutral wind at 400 km altitude has also been found to exhibit wave-4 longitudinal variation [*Häusler et al.*, 2007], whose formation was suggested to be due to DE3 tides. Given either the close relation between EMA and EIA via ion drag or the internal relation between neural density and wind via pressure gradient, it does not seem far-fetched to speculate that the neutral density and the EMA should also experience similar longitudinal modulations as in other quantities. Thus, our purpose in this study is to identify such signatures and to investigate its possible exciting agents.

2. Data

We utilize the thermospheric density and electron density data obtained simultaneously from the CHAMP spacecraft, which is in a near-circular orbit with an inclination of 87.3° and an initial height of $\sim$450 km at launch in July 2000. It probes the in-situ thermospheric density with a tri-axial accelerometer and the in-situ electron density with a Planar Langmuir probe. Readers can refer to *Liu et al.* [2006] and *McNamara et al.* [2007] for details concerning the derivation procedure and accuracy of the data.

In view that both EMA and EIA structures are more prominent around equinoxes at high solar flux levels [*Liu et al.*, 2007], we choose data during March-April 2002 and Aug.-Sept 2002 for the analysis that follows. Data under quiet conditions (Kp$\leq$ 3) are used. Both electron and neutral densities have been normalized to a common height of 400 km, using the NRLMSISE-00 [*Picone et al.*, 2002] and IRI2000 model [*Bilitza*, 2003]. These data are then binned with 5° latitude$\times 10^\circ$ longitude grids in geographical coordinates.

3. Results

Global distributions of the electron density and neutral density in geographic coordinates are presented in Figure 1. These are average patterns between 14–18 LT, when the EMA structure is prominent. Solid lines depict the dip equator. **Figure 1**

The electron density in Figure 1a shows the familiar EIA structure, with a wave-4 longitudinal modulation of crest density peaking near 0°E, 90°E, 180°W, and 80°W. This feature has been observed from various satellites like IMAGE, Formosat3/COSMIC, and CHAMP [*Immel et al.*, 2006; *Lin et al.*, 2007; *Liu and Watanabe*, 2008].

Meanwhile, the neutral density (Figure 1b) exhibits a prominent EMA structure, with a trough at the equator and density crests near $\pm 25°$ dip latitudes. A pronounced 4-peak longitudinal modulation similar to that in the EIA is clearly visible. It has three distinct density maxima around $20°$W, $70°$E, $130°$E, and a less obvious maximum around $130°$W, with slight hemispheric asymmetry. Note that these EMA peaks are somewhat shifted in location from those of the EIA.

To examine the longitudinal variation in more detail, densities in the trough and crest regions are extracted. Trough densities are obtained by averaging densities within $\pm 5°$ dip latitudes, while crest densities are averages over both hemispheres within [$\pm 10°$ $\pm 20°$] dip latitudes for the EIA and [$\pm 20°$ $\pm 30°$] dip latitudes for the EMA. Results are shown in Figures 2a and 2b. **Figures 2** Evidently, EIA trough and crest densities both display a prominent 4-peak structure, which are anti-phase to each other. This is easily understood, given that EIA is driven by the equatorial fountain process. The EMA also exhibits a pronounced 4-peak modulation in both trough and crest regions. However, unlike in the case of EIA, these modulations are rather matching each other quite well in phase. Note that using geographic latitudes for this analysis leads to the disappearance of the wave-4 in the EIA, and a significant weakening of it in the EMA. This is expected because both EIA and EMA are closely aligned with the dip equator as seen in Figure 1 and discussed in *Liu et al.* [2007]. Dip latitudes should be used to best extract the wave-4 feature in the crest and trough regions.

It is worth noting that the four peaks of EMA are somewhat displaced in longitude from those of EIA. To quantify this displacement, a Fourier transformation is applied to the curves in Figures 2a and 2b. The synthesized wavenumber 4 component is shown in Figures 2c and 2d. The peak-to-peak amplitude in the EIA crest/trough is about 2×10^5 cm^{-3}/1.5×10^5 cm^{-3}, corresponding to approximately 10$\pm 0.05\%$ of the background electron density. The amplitude in EMA has an amplitude about 0.15×10^{-12} kg m^{-3}, corresponding to 2$\pm 0.2\%$ of the background neutral density. We see that in the crest region, the EIA and EMA wave-4 variations are largely displaced to each other. In the trough region, however, they are nearly in phase, and the EMA peaks at about 10° east to the EIA.

4. Discussion

Results presented above provide a fairly clear picture of a marked 4-peak longitudinal modulation of the EMA, in reminiscence of that in the EIA. Several interesting features are discussed below.

First, wave-4 like modulations in EMA crest and trough region are in phase with each other, while those in EIA are perfectly anti-phase to each other (Figures 2a, 2b). This anti-phase relation in EIA trough and crest can be understood as a straightforward effect of the equatorial fountain process which drives EIA. This process removes plasma from the EIA trough region and transports it to the EIA crest region. Thus, the anti-phase relation provides strong evidence for the suggested DE3 tidal modulation of the E-region dynamo [*Hagan et al.*, 2007; *Jin et al.*, 2008]. In contrast, the EMA's crest and trough exhibt in-phase longitudinal modulation. This difference between the EMA and EIA clearly disqualifies the EIA as a major cause for EMA's wave-4 modulation via ion drag. It is because if ion drag were the cause, the longitudinal structure of EMA should mirror that of the EIA, with the wave-4 pattern in the EMA crest and trough being anti-phase to each other. Therefore, the in-phase relationship between the EMA crest and trough strongly precludes any significant contribution from EIA's wave-4 structure to the EMA's wave-4 longitudinal modulation.

With the in-situ exciting agent of ion drag being excluded, due consideration needs to be paid to the direct upward propagation of the tidal component DE3. One possibility is the direct penetration to F-region heights, which can potentially impinge a wave-4 structure on upper thermospheric quantities [*Oberheide and Forbes*, 2008b]. Our results show that the wave-4 in the EMA peaks around $30°$W longitude and those separated $90°$ apart (Figures 2c, 2d). In the light that wave-4 in the equatorial zonal wind at 16 LT peaks around $15°$W [*Häusler and Lühr*, 2009], we obtain a $15°$ longitude difference between the neutral density and wind, which translates to a phase difference of 4 hours. This observed density-wind phase lag finds good agreement with theoretical predictions by *Oberheide et al.* [2009] about the DE3-induced neutral density and wind perturbations at 400 km. Furthermore, our analysis reveals a $2{\pm}0.2\%$ peak-to-peak amplitude in the wave-4 variation of the neutral density, which is again very close to the predicted value of 1.8-2% in *Oberheide et al.* [2009]. Therefore, these agreements between observations and predictions give strong supporting evidence for a direct upward propagation of DE3 to F-region heights. Another process via the DE3-induced wave-4 structure in NO composition in the lower thermosphere [*Oberheide and Forbes*, 2008a] may contribute as well. Since NO acts as the atmosphere's natural thermostat via its 5.3 μm emission [*Mlynczak et al.*, 2007], its wave-4 variation might potentially affect the Earth's upper thermospheric energy budget. Note that in comparison to the route via E-region dynamo process, which has induced a disturbance with peak-to-peak amplitude of $\sim$10% in the F-region electron density, direct penetration or via NO has caused only $\sim$2% disturbances in the neutral density.

To conclude, the EMA exhibits a pronounced wave-4 longitudinal pattern which results more likely from the direct impacts of DE3 than from the EIA via ion drag. This wave-4 pattern in the neutral density shows a 4-hour phase difference from the wave-4 pattern in the zonal wind, which is consistent with theoretical predictions. We may envisage the following. The DE3 penetrates upward and first reaches E-region heights, where it modulates the E-region dynamo and consequently causes a wave-4 structure in the EIA when observed at constant local time. The DE3 continues to penetrate upward and reaches F-region heights, where it impinges a wave-4 signature in the neutral density and wind, but with a 4-hour phase difference. All these observations add further evidence for the influence of deep convection in the tropical troposphere on the thermospheric dynamics.

Acknowledgments. We thank Prof. T. Nakamura for interesting discussions and Dr. S. Thampi for careful reading the manuscript. The work of HLiu is supported by the JSPS foundation. The CHAMP mission is supported by the German Aerospace Center (DRL) in operation and by the Federal Ministry of Education and Research (BMBF) in data processing.

References

Appleton, E. V. (1946), Two anomalies in the ionosphere, *Nature*, *157*, 691.

Balan, N., and G. J. Bailey (1995), Equatorial plasma fountain and its effects: Possibility of an additional layer, *J. Geophys. Res.*, , *100*, 21,421–21,432, doi:10.1029/95JA01555.

Bilitza, D. (2003), International reference ionosphere 2000: Examples of improvements and new features, *Adv. Space Res.*, *31*, 757–767.

Hagan, M. E., A. Maute, R. G. Roble, A. D. Richmond, T. J. Immel, and S. L. England (2007), Connections between deep tropical clouds and the Earth's ionosphere, *Geophys. Res. Lett.*, *34*, L20109, doi:10.1029/2007GL030142.

Häusler, K., and H. Lühr (2009), Nonmigrating tidal signals in the upper thermospheric zonal wind at equatorial latitudes as observed by CHAMP, *Ann. Geophys.*, *27*, 2643–2652.

Häusler, K., H. Lühr, S. Rentz, and W. Köhler (2007), A statistical analysis of longitudinal dependences of upper thermospheric zonal winds at dip equator latitudes derived from CHAMP, *J. Atmos. Solar-Terr. Phys.*, *69*, 1419–1430.

Immel, T. J., E. Sagawa, S. L. England, S. B. Henderson, M. E. Hagan, S. B. Mende, H. U. Frey, C. M. Swenson, and L. J. Paxton (2006), Control of equatorial ionospheric morphology by atmospheric tides, *Geophys. Res. Lett.*, doi:10.1029/2006GL026161, l15108.

Jin, H., Y. Miyoshi, H. Fujiwara, and H. Shinagawa (2008), Electrodynamics of the formation of ionospheric wave number 4 longitudinal structure, *J. Geophys. Res.*, *113*, A09307, doi: 10.1029/2008JA013301.

Lin, C. H., et al. (2007), Plausible effect of atmospheric tides on the equatorial ionosphere observed by the FORMOSAT-3/COSMIC: Three-dimensional electron density structures, *Geophys. Res. Lett.*, *34*, L11112, doi:10.1029/2007GL029265.

Liu, H., and S. Watanabe (2008), Seasonal variation of the longitudinal structure of the equatorial ionosphere: Does it reflect tidal influences from below?, *J. Geophys. Res.*, *113*, A08315, doi:10.1029/2008JA013027.

Liu, H., H. Lühr, V. Henize, and W. Köhler (2005), Global distribution of the thermospheric total mass density derived from CHAMP, *J. Geophys. Res.*, *110*, A04301, doi:

10.1029/2004JA010741.

Liu, H., H. Lühr, S. Watanabe, W. Köhler, V. Henize, and P. Visser (2006), Zonal winds in the equatorial upper thermosphere: decomposing the solar flux, geomagnetic activity, and seasonal dependencies, *J. Geophys. Res.*, *111*, A09S29, doi:10.1029/2005JA011415.

Liu, H., H. Lühr, and S. Watanabe (2007), Climatology of the Equatorial Mass Density Anomaly, *J. Geophys. Res.*, *112*, A05305, doi:10.1029/2006JA012199.

McNamara, L., D. L. Cooke, C. E. Valladares, and B. W. Reinisch (2007), Comparison of CHAMP and Digisonde plasma frequencies at Jicamarca, Peru, *Radio Science*, *42*, doi: 10.1029/2006RS003491.

Mlynczak, M. G., et al. (2007), Evidence for a solar cycle influence on the infrared energy budget and radiative cooling of the thermosphere, *J. Geophys. Res.*, A12302, doi: 10.1029/2006JA012194.

Oberheide, J., and J. Forbes (2008a), Thermospheric nitric oxide variability induced by nonmigrating tides, *Geophys. Res. Lett.*, *35*, L16814, doi:10.1029/2008GL034825.

Oberheide, J., and J. Forbes (2008b), Tidal propagation of deep tropical cloud signatures into the thermosphere from TIMED observations, *Geophys. Res. Lett.*, *35*, L04816, doi: 10.1029/2008GL032397.

Oberheide, J., J. Forbes, K. Hausler, Q. Wu, and S. L. Bruinsma (2009), Tropospheric tides from 80-400 km: propagation, inter-annual variability and solar cycle e?ects, *J. Geophys. Res.*, doi:10.1029/2009JD012388, in press.

Picone, J. M., A. E. Hedin, D. P. Drob, and A. C. Aikin (2002), NRLMSISE-00 empirical model of the atmosphere: Statistical comparisons and scientific issues, *J. Geophys. Res.*, *107*, 1468, doi:10.1029/2002JA009430.

Sagawa, E., T. J. Immel, H. U. Frey, and S. B. Mende (2005), Longitudinal structure of the equatorial anomaly in the nighttime ionosphere observed by IMAGE/FUV, *J. Geophys. Res.*, *110*, A11302, doi:10.1029/2004JA010848.

Wan, W., L. Liu, X. Pi, M.-L. Zhang, B. Ning, J. Xiong, and F. Ding (2008), Wavenumber-4 patterns of the total electron content over the low latitude ionosphere, *Geophys. Res. Lett.*, doi:10.1029/2008GL033755, l12104.

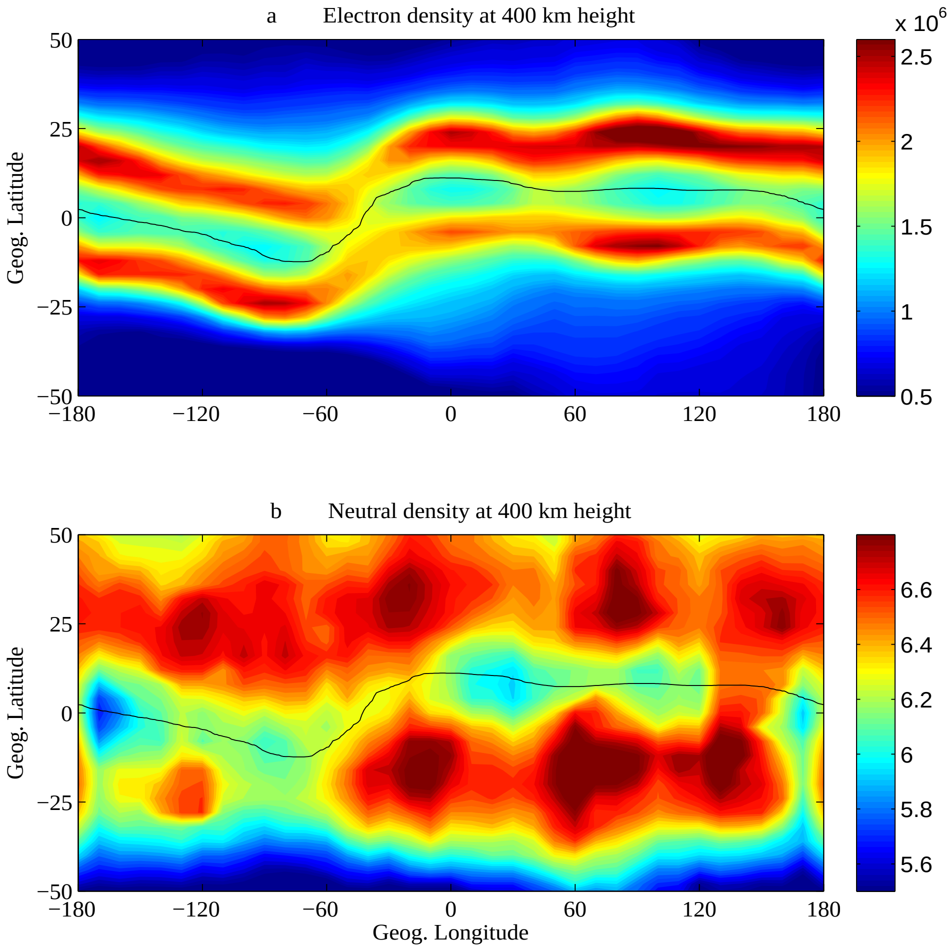

Figure 1. Distribution of the electron density (a. in unit of cm^{-3}) and neutral density (b. in unit of 10^{-12} kg) during 14–18 LT in the geographic coordinates near equinoxes in 2002.

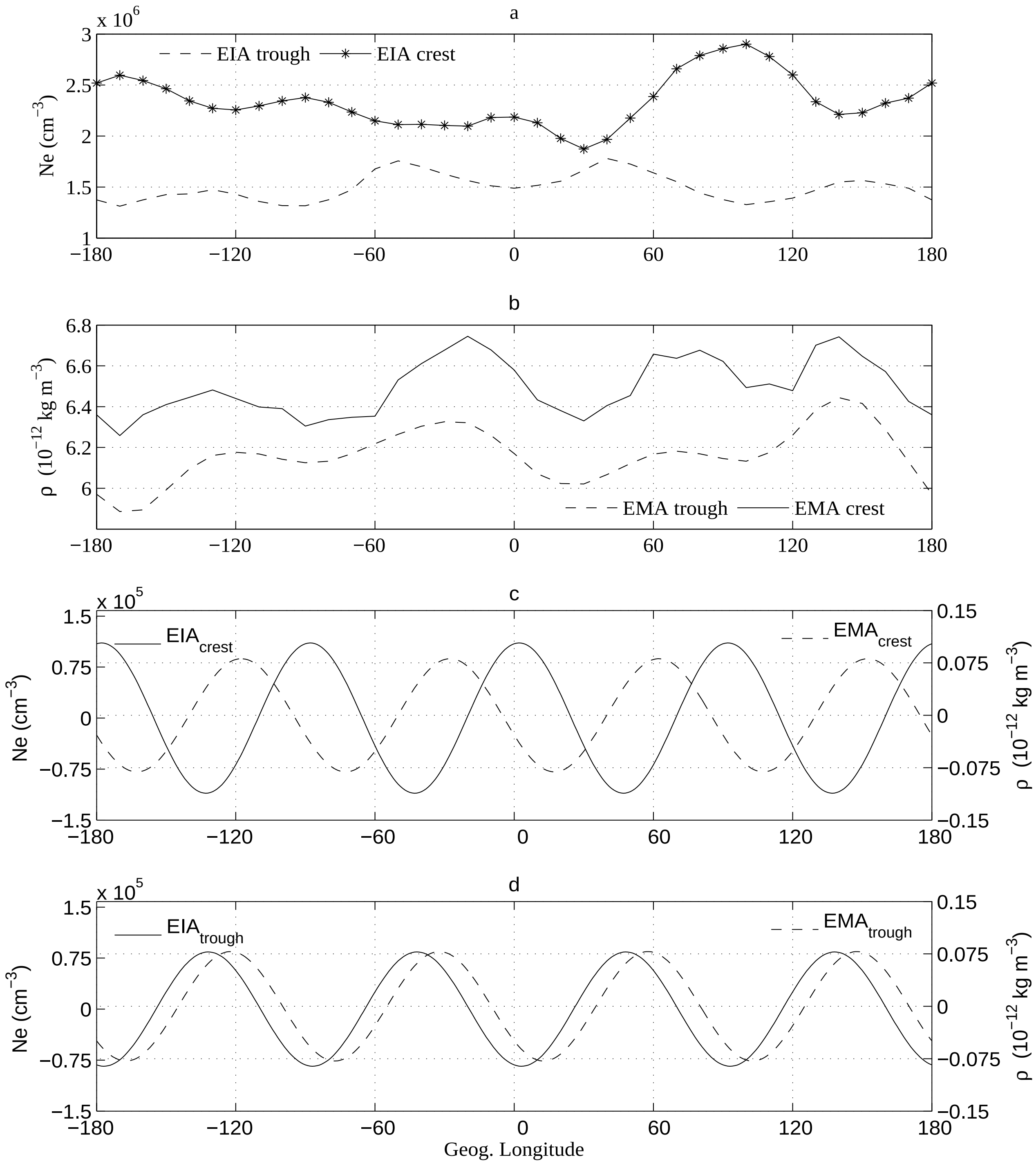

Figure 2. Longitudinal variation of the electron and neutral density in the trough and crest regions, along with their synthesized wavenumber 4 component.